RESEARCH ARTICLE

ADVANCED
ELECTRONIC
MATERIALS
Open Access

www.advelectronicmat.de

Soft Electronic Switches and Adaptive Logic Gates Based on Nanostructured Gold Networks

Giacomo Nadalini, Alexander Dallinger, Davide Sottocorno, Francesco Greco, Francesca Borghi,* and Paolo Milani

The advent of neuromorphic substrates is promoting the development of in materia autonomous and adaptive devices, employed as hardware solutions to reduce the current inefficiencies of traditional data processing techniques, in terms of energy requirements. The integration of data processing capabilities on soft materials is here focused on the development of the edge computing paradigm of interest for soft robotics and wearable devices. For such purposes, gold nanostructured complex networks produced in the gas phase are employed to fabricate neuromorphic devices. The integration of the latter on a soft Polydimethylsiloxane (PDMS) substrate equipped with stretchable laser-induced graphene electrodes, is exploited for the production of in materia devices to bridge the gap between data processing and interaction with the environment. The description and the control of the non-linear, resistive switching electrical properties are demonstrated by the development of soft mechano-responsive electronic switches and soft reconfigurable logic gates. These preserve Boolean functions classifications even under small mechanical perturbations, thanks to the redundant and adaptive connectivity of the gold networks. These results constitute a promising starting point for a fruitful combination of physical and computing intelligence directly integrated on soft systems to efficiently interact with the surrounding scenario.

1. Introduction

Living systems can efficiently interact with and adapt to the environment[1,2] through data processing mechanisms resulting from an adaptive physical substrate[3] and an efficient platform of sensory-motor integration.[4] Artificial systems aiming to mimic such efficient autonomous interaction capabilities should be characterized by the deep integration of information processing units and energy transduction ones, with sensors and actuators embedded and distributed within a soft body[5] able to implement its adaptive functionalities which could be used for computation in response to the sensorial perceiving.[6]

Bio-inspired soft robotics has made substantial progress thanks to the development of engineered functional flexible/stretchable materials, soft actuators, and their integration with high-resolution and sensitivity sensors.[6] To improve the data processing capability and the adaptability of soft embodied intelligent systems to external stimuli,[2,3] a major bottleneck is represented by the need to integrate bulky electronic control systems with high power consumption and/or to transmit high amount of data to remote processing units, thus severely limiting autonomy and adaptability to the environment.

To avoid huge data transfer to external processing hubs, the development of edge computing systems implemented in

G. Nadalini, F. Borghi, P. Milani
CIMaINa and Dipartimento di Fisica "Aldo Pontremoli"
Università di Milano
Milano 20133, Italy
E-mail: francesca.borghi@unimi.it

A. Dallinger, F. Greco
Institute of Solid State Physics
NAWI Graz
Graz University of Technology
Graz 8010, Austria

D. Sottocorno
Dipartimento di Fisica e Astronomia "Augusto Righi"
Università di Bologna
Bologna 40126, Italy

F. Greco
The Biorobotics Institute and Dept. of Excellence in Robotics & AI
Scuola Superiore Sant'Anna
Pontedera 56127, Italy

F. Greco
Interdisciplinary Center on Sustainability and Climate
Scuola Superiore Sant'Anna
Pisa 56127, Italy

hardware solutions distributed as close as possible or even embedded in the robot body is actively pursued.[7] However traditional processing units based on von Neumann architectures have an intrinsic problem of high energy consumption[8] thus imposing a trade-off between power lifetime and computing capability.

Autonomy and adaptability requirements impose the need for a radical change of paradigm in terms of hardware and software for data processing units that must fit a soft embodiment in shape-changing structures undergoing frequent reconfiguration to face rapidly changing and often unpredictable tasks.[2]

This challenge is being addressed using programmable stimuli-responsive materials that use structural compliance for computation or passive adaptability.[9] However, autonomous systems capable of interact with complex environments should support a type of intelligence based on the integration of sensory feedback control and requiring sophisticated data management and processing capabilities on board based on digital logic and computation.[5]

In pneumatically actuated soft robots, digital logic gates exhibiting functional completeness have been fabricated by using soft components.[10] Although this approach allows the execution of complex functions, the use of pneumatic components hampers the autonomy of the system, and the ability to perform advanced operations requiring a huge number of logic gates is substantially limited by the difficulty of combining many soft valves on the same platform.

Another approach to the integration of digital logic gates on soft and compliant systems is the fabrication of electronic devices on flexible substrates,[11–13] but functioning under mechanical stimuli is far from being demonstrated and no stretchable devices have been produced.

During the last decade, Supersonic Cluster Beam deposition (SCBD) has been reported as an additive manufacturing technique based on the gas-phase generation of cluster beams and in their controlled deposition on soft polymeric substrates for the production of compliant electrodes,[14] sensors,[15] actuators[16] and energy storage devices.[17,18] Recently we have also reported the fabrication of neuromorphic devices by assembling gold clusters via SCBD on silicon and glass substrates[19] as reconfigurable Boolean function classifiers,[20,21] which exploit the reorganization at the nano and meso-scale of the high defects dense and nanogranular cluster-assembled metallic network due to the current-driven mechanisms.[22–25]

Here we demonstrate a soft nanostructured device,[26,27] obtained by implanting gold clusters via SCBD in a Polydimethylsiloxane (PDMS) matrix, which is a stretchable and flexible insulator material,[28] with embedded Laser-Induced Graphene (LIG) electrodes.[29] After an electrical forming process, the gold-PDMS nanocomposite (ns-Au/PDMS) shows a non-linear electrical behavior with resistive switching (RS) activity, already described for ns-Au/SiOx devices.[22,23] These soft devices exploit the redundant and adaptive structure of gold nanostructured networks to realize reversible electronic switches and reconfigurable logic gates; a single device can generate all the 2-bit and most of the 3-bit logic gates. We tested the electric behavior and stability of the ns-Au/PDMS devices against unidirectional mechanical deformation.

2. Experimental Section

2.1. Embedded Laser-Induced Graphene Electrodes

The stretchable electrodes used as a substrate for the gold particle deposition were created by embedding LIG into PDMS. LIG is a nanoporous, crystalline carbon material created by laser-induced pyrolysis of polymer precursors. It is composed of defective graphene sheets that are randomly stacked and oriented, resulting in the formation of a porous network.[29] When LIG is embedded in a soft stretchable matrix it enables the fabrication of stretchable conductors with tunable piezoresistive response, usually exploited for strain sensors.[30–32] In particular, the application of longitudinal strain increases the spacing between the graphene sheets thus lowering the number of contact points between these, resulting in a specific resistance increase for the graphene networks.[30] The possibility to tune the piezoresistive response in this materials arises from the flexibility of the LIG electrode production technique, which allows for the creation of LIG electrodes with different densities. The custom LIG patterns were laser scribed onto a polyimide (PI) tape (Kapton HN, thickness = 50 μm, with silicone glue, supplied by M&S Lehner GmbH) fixed onto a glass slide (25 × 75 × 1 mm, ISO 8037/1, Epredia). A laser cutter/engraver (Universal Laser Systems VLS 2.30, Power 30 W) operating with a CO_2 laser source at 10.6 μm wavelength and equipped with an HPDFO (High-Power Density-Focusing Optics) beam collimator (nominal beam size in focus: 25.4 μm) was used to create LIG conductive patterns. The following settings of laser rastering parameters were employed for producing LIG-P:[32] $P = 10\%$, $S = 10\%$, raster resolution of 500 PPI, image density (ID) of 5 (arbitrary scale, defining a spacing between consecutive rastered lines of ≈50 μm), and a positive defocusing of $Z = 0.1$ mm. The laser scribing orientation was parallel to the elongated dimension of the electrodes.

The PDMS substrates were prepared by spin coating a 100 μm thick layer of polymer precursor (Sylgard 184 Silicone Elastomer Kit from Dow Corning, mixed in a 10:1 ratio) on a 47 PI film equipped with LIG electrodes, at 600 rpm for 60 s. The polymer was then cured by heating at 80 °C for 2 h, after a degassing process which eliminates residual air bubbles formed during mixing and pouring the polymer precursor on the substrate. After complete curing the PDMS/LIG electrodes were peeled off from the PI substrate with the help of a solvent-induced swelling. The samples were placed in a glass petri dish and the bottom of the petri dish was filled with n-Hexane (CAS No.: 110-54-3) and a lid was placed on top. After a few minutes, the PDMS started swelling and the PDMS/LIG electrodes could be easily peeled off from the substrate. The electrodes were then soaked in deionized water and dried on a heating plate at 100 °C for several minutes. The procedure of making PDMS/LIG electrodes is illustrated in **Figure 1**a.

2.2. Cluster-Assembled Thin Films

A SCBD apparatus, Figure 1b, equipped with a Pulsed Micro Plasma Cluster Source (PMCS)[33,34] was employed to fabricate the devices based on nanostructured Au implanted in PDMS substrates. Au clusters were produced in the gas phase through the PMCS thanks to the ignition of a high-pressure inert gas (Ar)
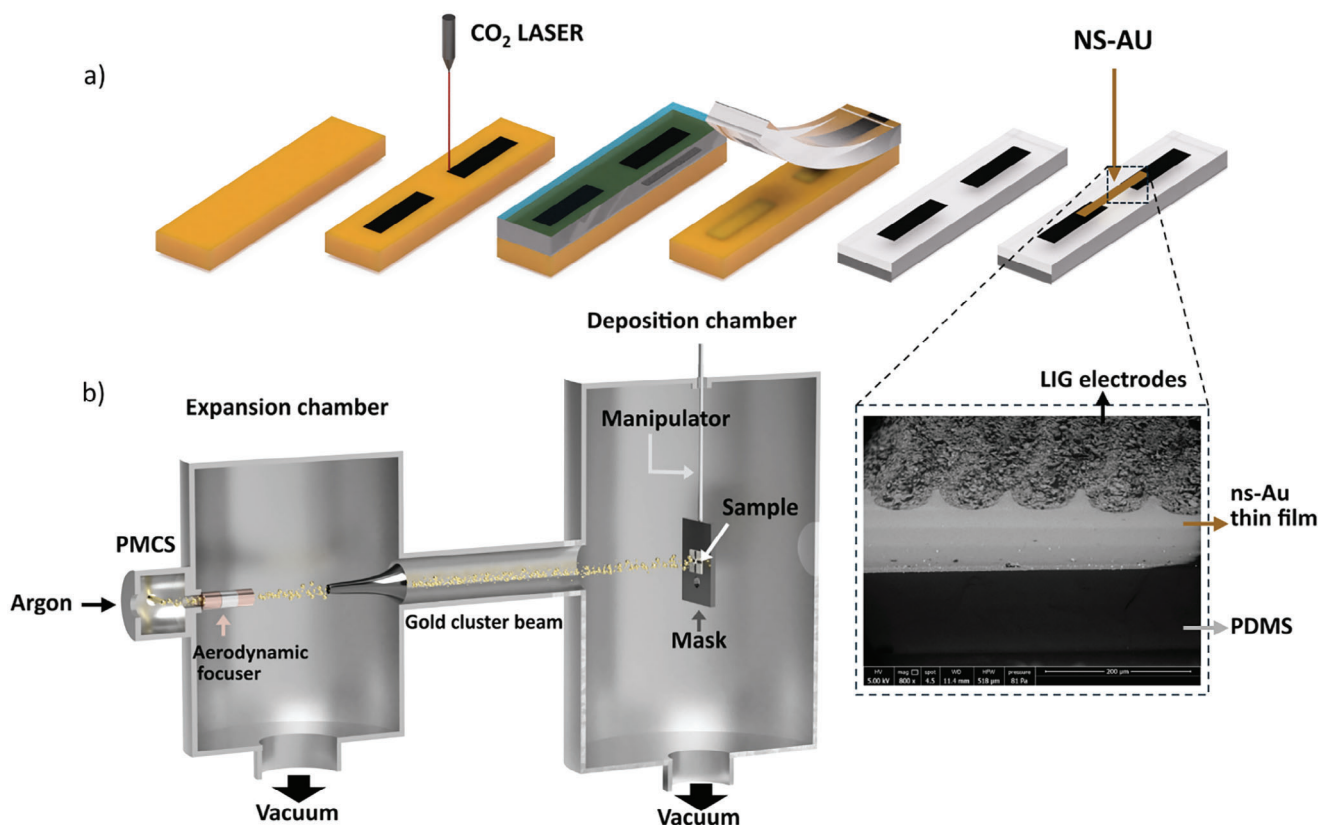
ADVANCED
SCIENCE NEWS

www.advancedsciencenews.com

ADVANCED
ELECTRONIC
MATERIALS

www.advelectronicmat.de

Figure 1. a) Schematic representation of the different steps for the fabrication of a PDMS substrate equipped with stretchable LIG electrodes. From left to right: Polyimide (PI) substrate; PI substrate with LIG electrodes scribed by CO_2 ($\lambda = 10.6$ μm) laser; embedding of the LIG electrodes into PDMS and polymer crosslinking; peeling off the PDMS substrate with embedded LIG electrodes; PDMS substrates equipped with LIG electrodes ready for ns-Au implantation by SCBD; two electrodes device obtained after SCBD of gold clusters bridging the two LIG electrodes b) Schematic representation of the SCBD apparatus (not to scale). On the left, the gold clusters are produced by the PMCS before being expanded in a supersonic beam. The beam is shaped by an aerodynamic focusing lens system in the expansion chamber before reaching the deposition chamber where clusters are implanted in the polymeric substrate which is properly mounted and masked on the sample holder attached to the manipulator. On the right, SEM image of the ns-Au/PDMS/LIG interface in oblique section view.

pulse followed by a high voltage electrical discharge resulting in the ablation of a gold target.[34] The ablated species thermalize with inert gas and condense to form clusters, the inert gas-clusters mixture is extracted from the source by the expansion through a nozzle into a vacuum (expansion chamber) generating a supersonic seeded beam. The cluster beam enters through a skimmer in the deposition chamber where it reaches the soft PDMS substrate fixed on a sample holder perpendicular to the beam trajectory.[33] A motorized holder permits the rastering of the substrate with respect to the beam allowing cluster implantation on an arbitrarily wide area. The neutral Au clusters reach the polymeric substrate with an energy of ≈0.5 eV/atom resulting in the penetration into the polymeric matrix of about a few hundreds of nm, while avoiding charging and carbonization of the substrate,[35] forming a nanocomposite layer.[14]

Two- and four-electrodes devices have been produced by implanting gold clusters by SCBD in the PDMS/LIG substrates. The gap between the two electrode devices was 1 mm, while the four-electrode devices consisted of a cross-like electrode geometry with a 1 mm squared gap in the center. The equivalent thickness of the implanted gold, namely the thickness deposited on a rigid control sample,[36] was ≈50 nm indicating that the amount

of deposited gold clusters is enough to build a sufficiently stable and complex network.

2.3. Electrical Characterization

Electrical characterizations were performed using a SMU (Keithley 2606B), both as a voltage source and for the current measurements, remotely controlled via homemade LabView programs to synchronize the application of the voltage and the measurement of the current at the desired sampling rate. The resistance R of the devices was obtained through Ohm's law R = V/I by applying a voltage V and measuring the current I in the device. In the case of current measurements at constant applied voltage, the current was sampled every 50 ms for several minutes (20 000 points, equivalent to 1000 s of total application time). The electrical characterization of the film was performed by means of repeated current measurements, with the ns-Au/PDMS samples biased by voltages varying according to a stepped triangular ramp (i.e., a piecewise input voltage) to derive the characteristic I–V curve of the two terminal devices. At each step of the voltage ramp, five consecutive measurements of the electric current were

**ADVANCED
SCIENCE NEWS**

www.advancedsciencenews.com

**ADVANCED
ELECTRONIC
MATERIALS**

www.advelectronicmat.de

repeated to ensure measurement reliability. Current compliances were imposed to control the switching behavior during the *I–V* curves collection, as reported in the next sections. In addition to constant voltage measurements, we used pulse measurements to study the effect of limited duration (10 ms period) stimuli on sample behavior, with a similar methodology as in ref. [37,38]. In literature this kind of pulsed measurements are often employed to characterize RRAM devices, where read and write pulses are used to monitor the resistive state of the sample and to control its stimulating switching phenomena, respectively. Two different types of pulses were used:

1) high positive or negative voltage pulses (write pulses), between 2 and 20 V, meant to change the resistance of the sample;
2) 0.1 V pulses (read pulses), to detect the non-volatile change of the conductive properties of the samples induced by write pulses.[37,38]

Multielectrode measurements were performed on four electrode devices to study the Boolean functions classification capability by means of the ns-Au/PDMS nanocomposites. The measurement setup, remotely controlled by ad-hoc LabView software, consists of a homemade extension of the Keithley 2606B Source Measurement Unit realized through the coupling with a relay matrix controlled by an Arduino board to switch between different electrodes couples. Digital inputs were provided applying 0 or 0.1 V between the input and the output electrodes while the output current was measured.

To classify the Boolean functions the analogic outputs were thresholded and digitalized in MATLAB environment, as previously reported for devices realized on rigid substrates.[39] Briefly, the model to which we refer is a nonlinear reconfigurable threshold logic gate, i.e., the Receptron model.[20,21,39] In the Receptron model the weights associated to the Boolean inputs are input-dependent, and not independent as in the Perceptron model.[21] This means that the outputs are not simply linear combinations of the inputs, and the associated weights are dependent, both in the theoretical model and in its hardware implementation.

In order to study which Boolean function a device can classify, 200 thresholds were applied to the analog outputs obtained after each writing step.[39] The procedure was repeated a few thousand times while the output electrode was cyclically changed, or rather each of the four electrodes was employed as the output electrode for a few hundred of writing steps.

2.4. Data Analysis

The analysis of the pulsed measurements and the characteristic *I–V* curves focused on the identification of the Resistive Switching (RS) events by means of ad-hoc MATLAB routines.

The RS data analysis of the measurements performed at constant applied voltage is extensively reported in ref. [22] and it was performed through software developed in MATLAB environment, aimed at identifying the electrical resistance temporal evolution. To distinguish between signal and noise in the case of a constant applied voltage, a threshold was established and compared to the relative difference of successive resistance values in the temporal resistance series. Therefore, two successive

resistance values are considered to be indicative of a switching event[22] if they differ more than four times the standard deviation of the resistance values computed within an interval without switching events, normalized by the average of the selected values. The analysis was carried out for each resistance series measured at different voltage values ($\pm$ 3, $\pm$ 5, $\pm$ 8 V). We computed the Inter-Switch-Interval (ISI) distribution by identifying the temporal distance $t_{ei} = t_{i+1} - t_i$ (the inter-event time) of consecutive switches for the entire interval of the recording series, in order to spot the presence of correlations of the switching events in the resistance time series.[40,41] The data are represented in the form of probability density distributions. We utilized the MATLAB-implemented least-squares method to fit the function that describes the distribution. In order to distinguish between correlated and uncorrelated resistance time series, which are represented by the aforementioned probability density functions, we fitted both power law and exponential functions and selected the best one by comparing the R^2 coefficients.[19] Time correlations can be identified by an ISI distribution that is the power law described, while uncorrelated time series are represented by a uniform distribution of switching events, i.e., an exponential trend.[40,42] To confirm the ISI evaluation and the presence of temporal correlations in sequences of discrete switching events, the analysis proposed by Karsai et al. in ref. [43] was performed. It consists of counting the switching events falling into a burst period $t_{ie} < \Delta t$, where Δt is a fixed time interval, longer than the inverse of the sampling frequency. Temporal correlations can be found by comparing the distributions of the number of events that occur within the same burst duration for original and shuffled data series. The uniform distribution of shuffled switching events will result in non-correlated behavior for the shuffled data series. Uncorrelated independent events in the shuffled data series are therefore represented by an exponential decay in the distribution data tail; conversely, a heavy tail described by a power law distribution indicates the presence of temporal correlation in the data.[44]

The resistance values distributions were computed and compared by means of the main statistical quantities to verify the null hypothesis through Welch's *t*-test, which was also tested on the obtained switching current, voltage, and power required to switch the resistive state to assess the most relevant quantities and thus the nature of the switching process.

2.5. Electro-Mechanical Characterization

The tensile mechanical investigation was conducted using a stepper motor-powered linear translator controlled by an Arduino board and MATLAB software. The samples were fixed by pressure clamps so that the 20 mm central region (called initial displacement L_0) was the only portion to be deformed. The employed clamps were made of copper in order to provide electrical contact with the PDMS/LIG electrodes. The strain (ϵ) was calculated as the ratio between the stand displacement ΔL and L_0. For each sample strains between 0.5% and 12.5% were explored, while different kinds of electrical measurements (*I–V* curves and train pulses) were performed at each elongation. Break tests were performed reaching strains up to 100%. The ns-Au/PDMS samples were investigated for multiple cycles by increasing stepwise
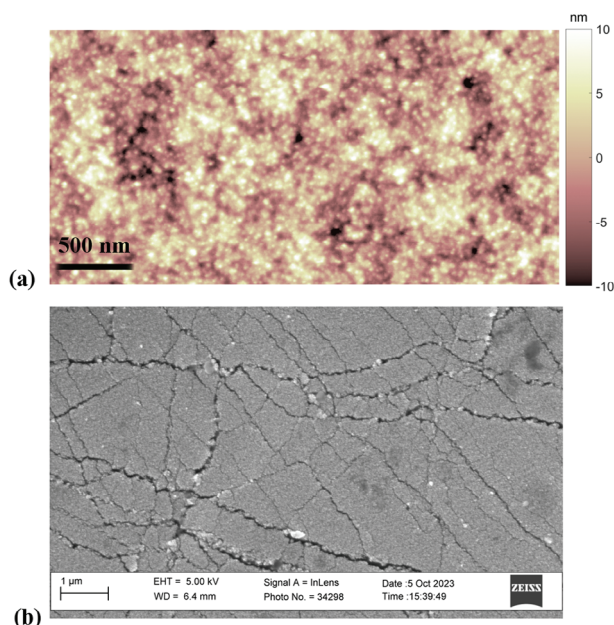
**ADVANCED
SCIENCE NEWS**

www.advancedsciencenews.com

**ADVANCED
ELECTRONIC
MATERIALS**

www.advelectronicmat.de

Figure 2. a) Atomic force microscopy image of the as-deposited ns-Au/PDMS surface; b) same sample scanned by SEM technique.

the elongation. After each elongation, the samples were brought back to the initial position L_0 to investigate the mechanical reset effect.

3. Results and Discussion

3.1. Gold Clusters Structure and Resistive Switching Forming Process

The as-deposited ns-Au/PDMS films showed rough interfaces (RMS roughness is ≈8 nm, **Figure 2a**), formed by interconnected nanometer-sized clusters[45] with a nanocrystalline structure[22] and a lot of defects, such as microstrains and stacking faults.[19] Despite the presence of cracks in the ns-Au/PDMS surface (see Figure 2b), the sample shows Ohmic behavior, with linear IV characteristics.

Similarly to what was observed on samples realized depositing gold clusters on rigid silicon substrates, the ns-Au/PDMS samples[19] required a forming process to trigger a reorganization of the network and the appearance of resistive switching electrical activity.[19] The procedure to trigger the RS activity consisted of applying a constant voltage, according to an increasing step-by-step procedure from a few V up to 40 V, for about a minute per voltage value, until an abrupt resistance increase was observed, as reported in Figure S1 (Supporting Information). The same figure reports a SEM image showing the modifications of the ns-Au network surface with an increase of the surface cracks density, specifically the ns-Au coverage of the PDMS surface decreases from 90% to 85% after the forming process. The parameters involved in the switching procedure closely resemble the ones used for ns-Au samples deposited on silicon-based substrates,[19] except for the lower current needed for the forming and thus the lower power required in the forming process. The structure of the gold matrix remains granular and full of grain boundaries

and defects at the nanoscale even after the forming process.[19] The role of such defects and boundaries in the reorganization of the granular network at the nano and mesoscale due to the current flowing through the device and the resulting RS activity have already been proved both experimentally and theoretically.[23–25,46] The resistance of the PDMS/LIG electrodes remained unchanged in response to the forming process as evidenced in Figure S2 (Supporting Information).

3.2. Resistive Switching Electrical Activity

Once the ns-Au/PDMS sample has been formed, the resistive switching activity recorded at constant applied voltage was characterized and analyzed according to the strategy described in the Experimental section. The nonlinear electrical behaviors of ns-Au/PDMS are comparable with the ones observed in ns-Au networks deposited on rigid substrates.[19,22] It has been extensively demonstrated how the RS activity takes place from the reorganization at the nano and meso-scale of the grain boundaries and defects characterizing such nanogranular structure due to current-driven local phenomena, as joule heating and electroforming processes.[22–24,46] The here reported ns-Au clusters networks are well beyond the percolation threshold, for this reason the RS activity can be attributed to the effects reported above. This is a remarkable difference with other RS devices employing gold nanoparticles in which the switching mechanism is based on tunneling between nanoparticles under the percolation threshold[47] or on filamentary related mechanisms.[48,49]

The RS event is identified as a resistance change greater than four times the noise level; in **Figure 3a** a typical resistive switching electrical behavior of the ns-Au/PDMS nanocomposite is shown. The RS activity was observed systematically for applied voltages greater than 2 V, even if some events were observed sporadically also for voltage of ≈0.5 V.

RS events, marked by red circles in Figure 3a, are grouped in burst periods followed by silence periods (no switching activity) of different durations. The RS time distribution was evaluated by means of the Inter Switch Interval (ISI) analysis, a tool described in the Material and Method section which is useful to indicate the presence of time correlation in the switching activity.[40,44] ISI distributions are presented in Figure 3b in logarithmic scale. The RS events grouped in small time windows contribute to the left side of the distribution, while the right side of the distribution considers the events separated by longer time periods, featuring the heavy tail in the distribution. The analysis was conducted on many time series acquired at different voltages on tens of samples. The computed distributions were fitted with power law and exponential line shapes to compare the R^2 coefficients and evaluate the best agreement, as also reported here.[19] The power law distribution manifests a heavy tail which indicates the presence of time correlations, while on the contrary the exponential distribution represents independent uncorrelated events.[50] To sustain such result the analysis proposed by Karsai et al,[43] reported in Materials and Methods, was conducted by computing the number of switching events belonging to intervals of 1 s. Karsai's analysis performed on both shuffled and unshuffled time series is reported in Figure 3c. For shuffled time series, the switching events are uniformly arranged and thus the resulting
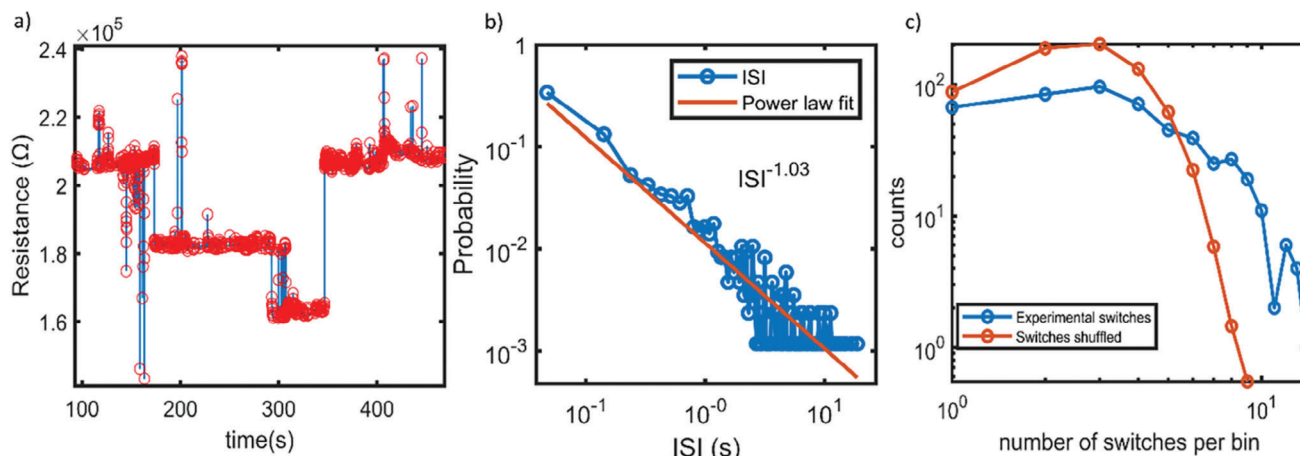
Figure 3. a) Resistive switching electrical activity at a constant applied voltage (8 V) showing multiple metastable resistance levels, the temporal evolution of the resistance is reported in blue, while red circles represent RS events. b) ISI distribution in log-log scale in blue and power law fit in orange, each point represents the probability to observe a certain time interval between two consecutive RS events. The comparison between the R^2 coefficients determines a better agreement with power law line shape compared to the exponential line shape ($R^2_{power\ law} = 0.84$; $R^2_{exponential} = 0.43$). c) Distribution of the number of RS per bin as proposed by Karsai:[43] in orange, the distribution of the shuffled resistance time series follows exponential trend while a heavier tail of the distribution of unshuffled data confirms the presence of time correlation in the spontaneous electrical activity.

number of events per time interval distribution does not show the tail expected for grouped events, as for the case of unshuffled ns-Au/PDMS samples data series which indicates the presence of correlations. Besides the scale-free dynamic characteristic highlighted by the ISI distribution, scale invariance properties are evidenced by the power law distributed resistance variations shown in Figure S3 (Supporting Information).

3.3. Bistable Resistance States

The electrical behavior of ns-Au/PDMS samples by means of IV curves is shown in **Figure 4**, which provides more hints on the switching nature of the samples.

In fact, the IV analysis highlighted the almost Ohmic conduction mechanism of the Low Resistance State (LRS), Figure 4a, while the High Resistance State (HRS), Figure 4b, it is evident its nonlinearity. The switching between HRS and LRS can be obtained by controlling the current compliance during IV curves. Multiple IV curves are shown in Figure 4a,b and in particular from Figure 4a it is possible to appreciate that the switch toward the HRS can happen at different values of the voltage ramps. This controllable protocol was investigated for up to 1000 cycles providing statistically relevant information on the parameters involved in the RS process. The HRS, identified in the range from 1 to 100 MΩ, differs from the LRS, identified in the range from 1 to 100 KΩ, by at least one order of magnitude for all the samples observed. Figure 4c shows the boxplots of the resistance value in the HRS and LRS, the current (Figure 4d), and the voltage (Figure 4e) required to trigger the switch between the two resistive states and the associated power (Figure 4f). In the legend of Figure 4 the *p*-values, at 5% significant level, associated to the test of the null-hypothesis between the couples are also reported. In particular, the null hypothesis was rejected for all the pairs of distributions except for the switching voltage. The fact that two well-defined distributions of electric current were observed

to switch the resistive state of the nanocomposites is a proof of the electric current relevance in this specific switching process. On the contrary, the electric voltage is not the key quantity of RS, since the two distributions of the switching voltage are not discriminated from each other. The recording of the IV curves in Figure 4 was performed at a scan rate of 10 V s^{-1} and no differences were observed by varying the scan rate as reported in Figure S4 (Supporting Information). The IV curve analysis indicates that the "macroscopic" RS between the HRS and LRS is an electric current-related process, allowing to use of current compliances in the IV curves to constrain the flow of specific electric currents in the nanocomposites facilitating the switching process, thus increasing the RS efficiency. Stability tests were performed on both the HRS and LRS resulting in the preservation of the resistive state for period of time up to 5 months, thus indicating that they are non-volatile resistance states, if neither mechanical nor electrical stimulations were applied.

3.4. Soft and Reversible Electronic Switches

The possibility to control the resistance state between the HRS and the LRS of devices based on PDMS-Au nanocomposite was investigated also by the employment of electrical pulses. Trains of five write pulses of voltage greater than 2 V were applied to the devices, followed by one reading pulse of 100 mV. Typically, the high resistance state (HRS) differs from the low resistance state (LRS) by more than one order of magnitude ($R_{on/off}$) (**Figure 5**). Five pulses of 5 V and 10 ms duration were employed to bring the sample in the HRS while five alternate pulses of ± 3 V were applied to reach the LRS. The change in voltage polarity of the different writing pulses was not strictly necessary but we obtained higher efficiencies employing alternate pulses to bring the samples in the LRS. This voltage polarity dependency may be ascribed to electromigration-related effects. We think that both current intensity and polarity are key features in the promotion of
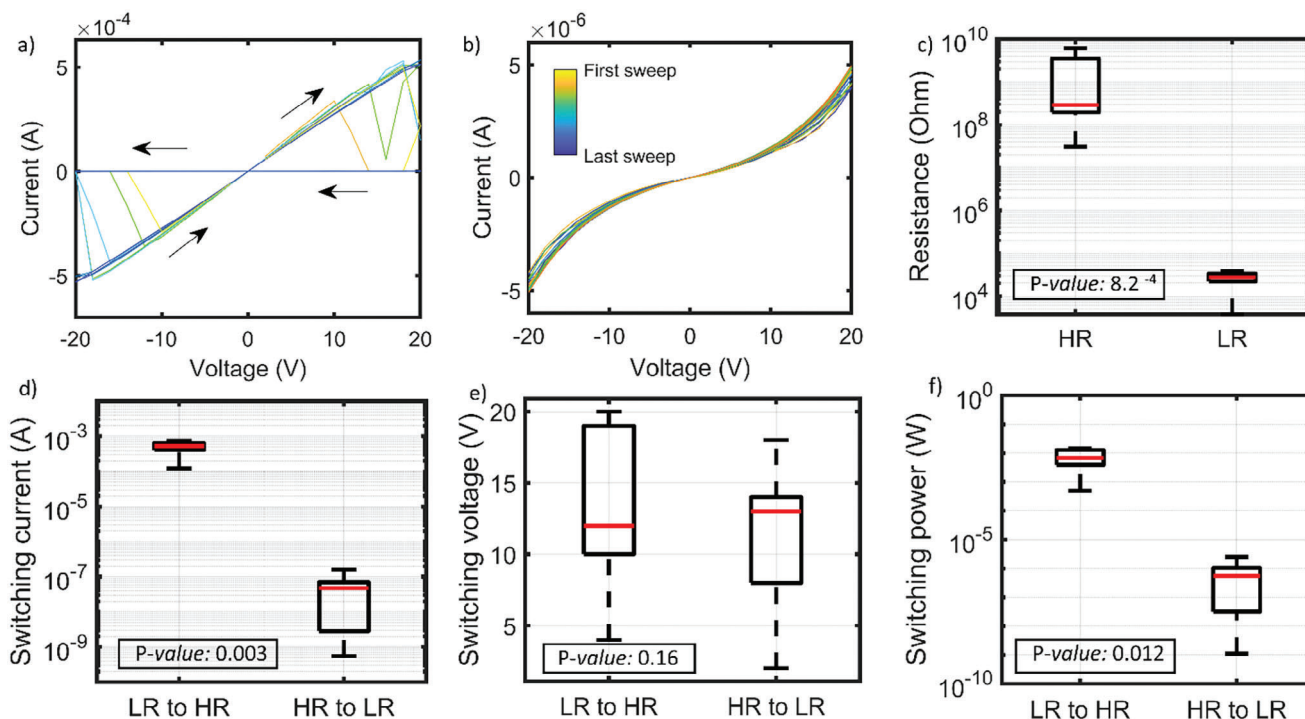
ADVANCED
SCIENCE NEWS

www.advancedsciencenews.com

ADVANCED
ELECTRONIC
MATERIALS
Open Access

www.advelectronicmat.de

Figure 4. a) The typical IV curves showing the nanocomposite switching between an almost linear LRS and a nonlinear HRS, RS events are easily recognizable as abrupt current variations. The arrows indicate the sweep direction and the various sweep cycles are represented according to the color-bar shared with b). b) Nonlinear IV characteristic of the HRS. c) Boxplot of the HRS-LRS values, the resistance is measured at 100 mV after each IV curve. d–f) Boxplots of the electric current, voltage, and power required to switch from one state to the other, respectively. In all the boxplots legends the p-values at 5% significance of the t-test of the null hypothesis are reported.

the on/off switch: the highest pulses of single polarity might induce local separation or deterioration of good interconnections of gold clusters in critical junctions inside the polymer matrix resulting in the reported overall resistance increase. Alternated lowest voltage pulses instead may restore such connections in junctions because of homogeneous local joule heating, leading to the observed resistance decrease. We tested the controlled resistive switching between HRS and LRS by means of electrical pulses for up to 3000 cycles.

The average electrical parameters obtained from these measurements are reported in **Table 1** in which the resistance states and the switching currents are specified; these values are in accordance with the ones obtained through the IV analysis reported previously. The efficiency of the switching process is also reported, indicating that the train of pulses are not always successful at the first test: sometimes the nanocomposite resistance remains unperturbed for a few cycles (e.g., Figure 5: seven consecutive cycles at ≈53 s in which the ns-Au/PDMS keeps the HRS).
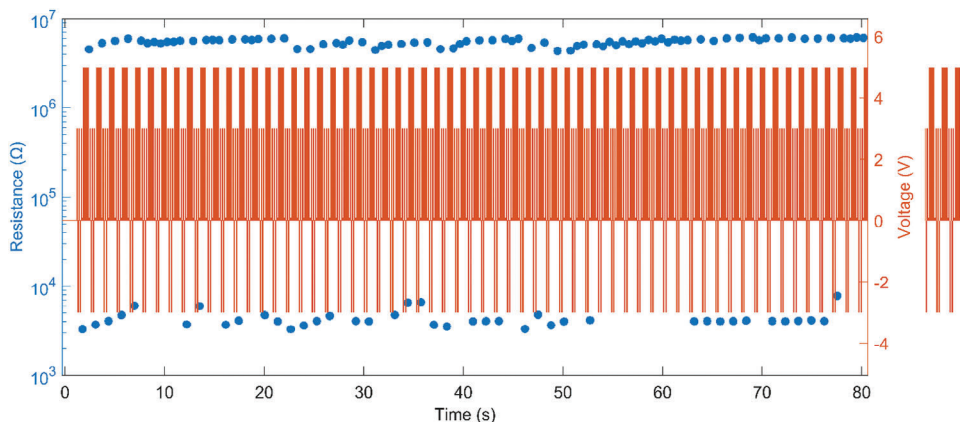

Figure 5. Pulsed voltage measurement in 80 s time window: consecutive trains of voltage pulses were applied to the nanocomposite and the electric current was subsequently measured. Orange vertical bars represent single voltage pulses while the blue dots represent the measured resistance value. Trains of five pulses were applied to bring the sample in the HRS and LRS, the current is measured at 0.1 V to compute the resistance value.

**ADVANCED
SCIENCE NEWS**

www.advancedsciencenews.com

**ADVANCED
ELECTRONIC
MATERIALS**

www.advelectronicmat.de

Table 1. The average value and standard deviation of the HRS and LRS are reported. I_{high} and I_{low} represent the average electric current necessary to bring the sample in the HRS and LRS, respectively. The efficiency of the switching process is reported too, as like the up and down efficiency which represents the efficacy of the train pulses to switch from the LRS to the HRS and vice versa, respectively.

	HRS [kΩ]	LRS [kΩ]	I_{high} [A]	I_{low} [A]	Efficiency	Up eff.	Down eff.
Average	10^4	4.5	0.0015	6^*10^{-7}	0.5	0.98	0.5
St. dev	7^*10^3	1.1	0.0004	3^*10^{-7}	0.1	0.02	0.1

The resistance state of the system can hence be controlled through a specific train of pulses input, which manages to modify the state of the adaptive network according to a non-deterministic manner, leading the system to two different conduction mechanisms.

3.5. Electro-Mechanical Characterization

The tensile mechanical analysis was conducted on the ns-Au/PDMS nanocomposites by stretching two electrode samples in one direction by means of a linear translator. The principal electrical response to the mechanical stimuli consists of a switch toward the HRS every time the sample length is varied above a strain value of 0.5%. The initial resistance state of the sample does not influence the trend described above, i.e., if the length of the nanocomposite is varied enough, the nanocomposite will reach the HRS. The observed switch to high resistance resulting from the applied strain is attributed to the ns-Au/PDMS because the resistance variation of the LIG electrodes is negligible compared to the changes observed in the resistance of the nanocomposites, as reported in Figure S5 (Supporting Information). Besides the effect of the strain on the electric resistance,

the response to different electrical stimuli such as IV curves was investigated to understand the effect of the stress on the resistive switching properties of the nanocomposite: the very same switching routine by IV curves with different current compliance demonstrated previously was performed at increasing strain values. The procedure consists of the application of repeated IV curves with alternating high and low current compliances (cc) respectively to bring the nanocomposite in the HRS and LRS, then each IV curve is followed by the measurement of the resistance at 100 mV.

Figure 6a reports the most frequent electrical response observed in the nanocomposites. At strain lower or equal to 0.5% the IV curves can switch the samples between the HRS and LRS because the cluster network is still dense enough to preserve electric conduction and resistive switching. At higher strain, the nanocomposite is stuck in the HRS because the cluster network density decreases bringing the nanocomposite in the HRS and preventing the switch to the LRS. It is important to note that for low strain values the possibility to switch the system between the HRS/LRS is still preserved and that even if the samples reach the HRS when strained, the possibility to switch between the two states is restored when the nanocomposites are brought back to the relaxed position. This is important evidence of the adaptability of the gold network embedded in the polymeric matrix, also to mechanical stimuli: by exploiting different local connectivity paths the system in rest position can restore its resistance state on both HRS and LRS, which would be otherwise impossible with a common electrode developed with deterministic connectivity.

Figure 6b–d reports the electric current, voltage, and power required to bring the sample from the HRS to the LRS (orange) and vice versa (blue) evidencing and corroborating the separation of the switching current and power values (blue and orange) which is not observable for the electric voltage case. The efficiency of the switching procedure based on IV curves is reported for each
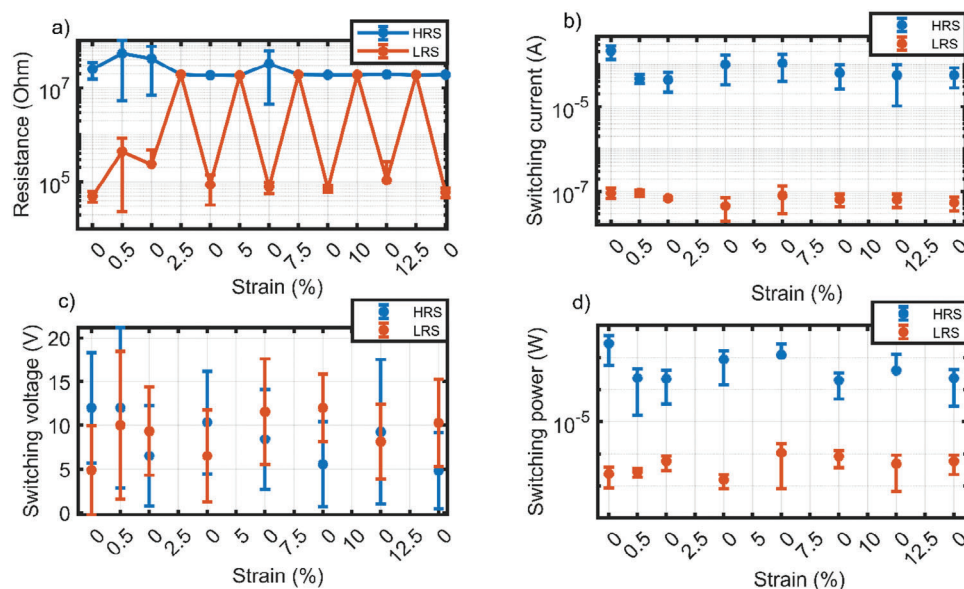

Figure 6. Resistive switching electric response probed by IV curves at increasing strain values alternated by rest positions. a) HRS and LRS measured after low cc and high cc, respectively. b–d) Electric current, voltage, and power required to switch the nanocomposite form the LRS to the HRS (blue) and vice versa (orange).

**ADVANCED
SCIENCE NEWS**

www.advancedsciencenews.com

**ADVANCED
ELECTRONIC
MATERIALS**
Open Access

www.advelectronicmat.de

elongation and each rest position in Figure S6 (Supporting Information). The data indicates that the IV curves in cc are not always successful on the first try but sometimes the resistance of the nanocomposites remains unperturbed for a few cycles. Figure S6 (Supporting Information) also describes the probability to observe the nanocomposite in the HRS or in the LRS during the switching procedure indicating that the ns-Au/PDMS is more likely to get stuck in the HRS.

The electromechanical behavior of the nanocomposites was tested for up to more than 200 elongation cycles, between 0% and 15% strain applied, confirming the results obtained in Figure 6. The endurance measurement is reported in Figure S7 (Supporting Information) highlighting the restoration of the ns-Au/PDMS RS functionality at rest position. The endurance measurements provided insights into the degradation of the nanocomposites with a drift toward the HRS. The aging can be ascribed to the quasi-3D cluster network reorganization resulting from the induced electromechanical perturbations. The latter modifies the metallic cluster network in a partially reversible manner promoting a variability in the electric response to the strain which may preserve the possibility to switch the resistance state or result in the collapse in a less conductive regime.

Good resilience was demonstrated by the nanocomposite during the break test (Figure S8, Supporting Information), in which even if the LIG electrode broke at 100% strain (in a region far from the ns-Au/PDMS), by mounting the sample back on stage it was still possible to switch between the HRS and LRS as before breakage.

3.6. Soft Reconfigurable Logic Gates

The fabrication of reconfigurable logic gates based on nanostructured gold cluster-assembled films deposited on rigid silicon substrates has been recently reported.[20,39] The device obtained by interconnecting a generic pattern of electrodes with a cluster-assembled Au film can perform the binary classification of input signals, following a thresholding process, to generate a set of Boolean functions.[39] Considering the non-linear conduction properties of cluster-assembled gold films and their non-local response to input signals,[20] a generalization of the perceptron model (named Receptron)[21] was proposed, where the input weights are input-dependent. Compared to the perceptron, a single Receptron is functionally complete[21] and not limited to the classification of linearly separable functions.[21,39]

In order to build reconfigurable logic gates, we exploited ns-Au/PDMS system with its nonlinear electrical properties, that closely resemble those observed in nanostructured Au films on silicon substrates.[22,23,45,51,52] In particular, multielectrode devices (**Figure** 7a) were realized to implement 2-bit and 3-bit logic gates. The cross-like geometry of the electrodes is bridged by the implanted Au clusters and it is schematically reported in the inset of Figure 7a. Given a certain distribution of electric resistances between the different electrode couples, the recording of the current outputs for each possible combination of the 2-bit or 3-bit system and the subsequent thresholding process, allows to reproduce a truth table, corresponding to a particular Boolean function.[39]

In a multielectrode device, the application of write pulses is exploited to modify the connectivity of the gold network and therefore the sequence of the outputs, giving rise to other Boolean functions.[20] Moreover, the complex connectivity and non-local electrical property of the cluster-assembled film prevent the output of to be a simple linear combination of the inputs: for example, the output current value for configuration 110 is not simply the combination between the output currents for 100 and 010 inputs[39] as in the case of a resistor network, but non-linear contributions appear when multiple input electrodes are electrically biased thus making possible the classification of non-linearly separable functions by a single device. The typical output distribution is reported in Figure 7b for 300 consecutive writing steps, where each writing step consisted of the random application of a train of pulses composed of five alternated ± 5 V pulses of 10 ms or ten unipolar 12 V pulses of 10 ms between random electrode couples providing a rich variability in the sequence of the outputs and an optimal function search efficiency, by confirming the efficacy of these train pulses also for multielectrode devices.[20,39] The effectiveness of the writing procedure is shown in Figure 7b from which it is possible to appreciate the outputs variability, particularly promoted at the 150th writing process, where each output sharing the input electrode number 3 manifested an electric current decrease of about a factor two. By choosing the right thresholds it was possible to easily implement the NAND or NOR 3-bit logic gates. The criterion for the selection of the threshold currents is the following: once all the outputs were measured, 200 evenly spaced thresholds were disposed between the maximum and minimum measured current values. It is important to note that the chosen thresholds were not changed over time. The number of functions generated by a single device is very high even if some 3-bit functions are not implemented after thousands of writing steps, as reported in Figure 7e) which graphically reports how many times each of the 256 3-bit Boolean functions were classified for all the writing processes. Nevertheless, the chance to classify the NOR and NAND logic gates gives the possibility to implement all the Boolean functions by simple combination respectively of only NOR or only NAND gates.[39] Moreover, it was demonstrated the capability to classify non linearly separable logic functions as the 2-bit XOR reported in Figure 7c employing a single device, the truth table is reported in Figure 7d. It was possible to generate all the 2-bit logic gates without the need of combining multiple devices and demonstrating the functional completeness of the device in the generation of Boolean functions, almost all for the 3-bit case.

The stability of the generated Boolean functions was investigated by reading multiple times (ten) the outputs after an idle time of 3 s between each reading cycle, without changing the threshold values. This procedure was repeated after each writing step. The observed variability in the output currents as a result of the writing phases is reported in the violin plots of **Figure** 8a for the different input combinations. The discrete variations observed in the violin plots represent the recurrent exploration of resistance levels separated by a certain value. This variability is qualitatively different as compared to the observed one during the reading phases (Figure 8b). In this case the variations are clearly of lower magnitude and do not show discrete frequent resistance changes as expected for a stable device.
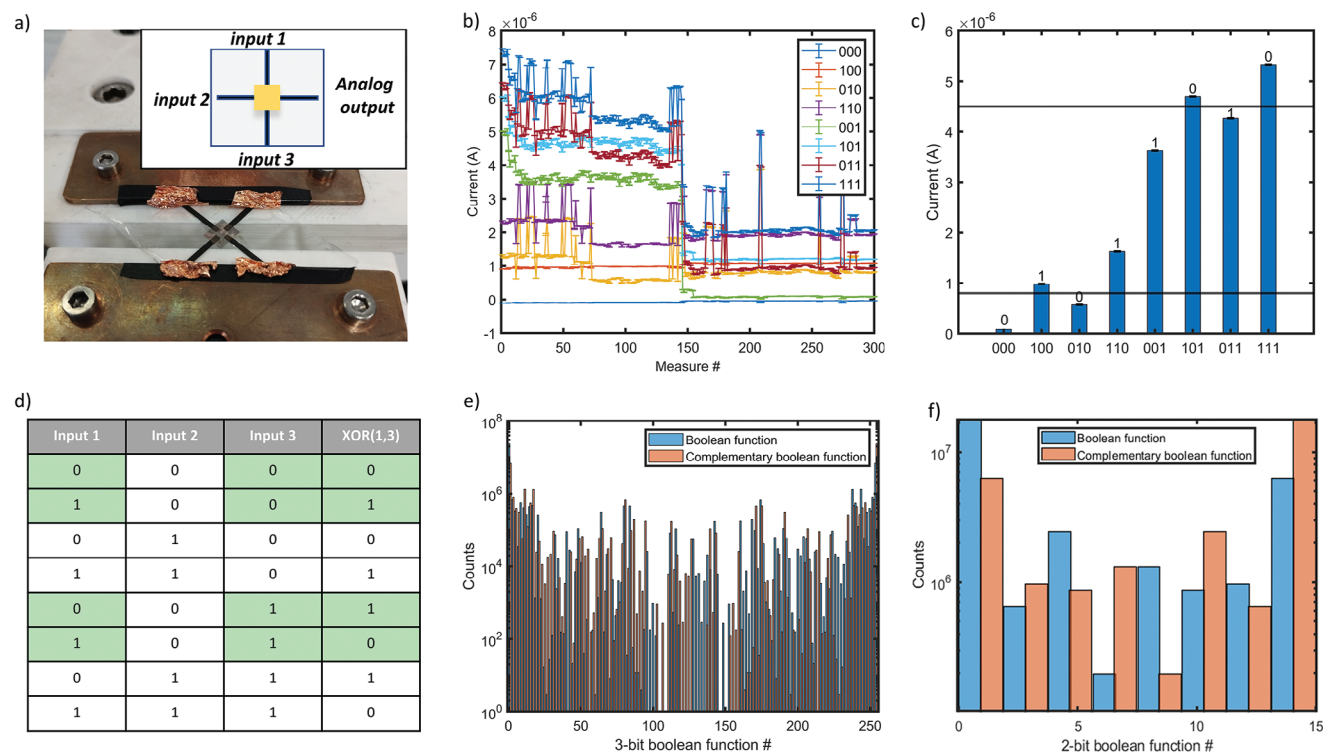
2400717 (9 of 12)

ADVANCED
SCIENCE NEWS

www.advancedsciencenews.com

ADVANCED
ELECTRONIC
MATERIALS

www.advelectronicmat.de

Figure 7. a) Image of a multielectrode device mounted on a linear translator. The black stripes in a cross-like geometry are the LIG/PDMS electrodes bridged by the Au clusters as schematically reported in the inset. b) Electric current measured for all the 3-bit input combinations after each of the 300 writing steps showing output variability over a broad range of resistances. c) Double thresholding of the output current at the 100th writing step shown in b), which classifies the 2-bit XOR logic gate considering electrodes 1 and 3; note that the effect of electrode 2 does not influence the classification of the 2-bit XOR function for electrodes 1 and 3, thus it can be completely neglected. The small error bars indicate that the device is noise-tolerant. d) Truth table of the 2-bit XOR logic gate for input electrodes 1 and 3. e,f) Histograms of all the 3-bit and 2-bit Boolean functions classified by means of one single device cycling through different output electrodes, the found functions and the complementary ones (which refer to the functions obtained by interchanging the 0 and 1 digital values above or below the thresholds) are reported in blue and orange, respectively.

The stability of the Boolean function generation was investigated under continuous mechanical perturbations. During the reading phases a cyclic mechanical deformation of 0.5% strain was imposed by mounting the devices on a linear translator (Figure 7a). The resulting variability is reported in Figure 8c from which a very similar behavior to the static case of Figure 8b is observed. The differences consist in the presence of some outliers in the variability distributions shown by means of the violin plots, and in an increase of the standard deviation of the distribution, reported in Figure 8d, for the different input combinations. Notably, even if the standard deviation increases from the static to the case under cyclic mechanical deformation, such increment is negligible compared to the variability induced by the writing phase (first column of Figure 8d). Moreover, the variability induced by the small deformations did not modify the Boolean functions distribution which is generated following the thresholding process. In fact, the percentage of lost Boolean functions during the mentioned stability measurements remains lower than 2.5% for both the static measurement and the ones under cyclic mechanical deformation.

This result demonstrates for the first time that it is possible to realize electrically reconfigurable logic gates[20,39] on soft, deformable, and biocompatible substrates as PDMS.

4. Conclusion

This work demonstrates the fabrication of a soft resistive switching device that can perform reconfigurable Boolean functions classification with an efficiency corresponding to functional completeness for 2-bit logic gates and close to it for 3-bit logic gates. The device was fabricated by Au clusters deposition on a PDMS substrate embedded with stretchable electrodes from Laser-Induced Graphene. The adaptability of the complex gold network, responsive to both electrical and mechanical stimuli, allows a reconfigurable, reversible, and controlled management of the device, which would be otherwise impractical with conventional logic gates printed on flexible substrates.

The ns-Au/PDMS nanocomposite showed stable LR and HR states and durable RS properties up to thousands of cycles, controlled by a combined approach based on voltage pulses and IV curves. The study of the response to IV curves provided information about the relevant parameters in the RS between the high and low resistance state, namely the current compliance in the IV curves to control the RS.

The adaptability of the network is proved by both the two-electrode and the multielectrode devices, which are thus able to integrate in a reversible and controllable manner the electric and mechanical stimuli, by means of the redundancy of the
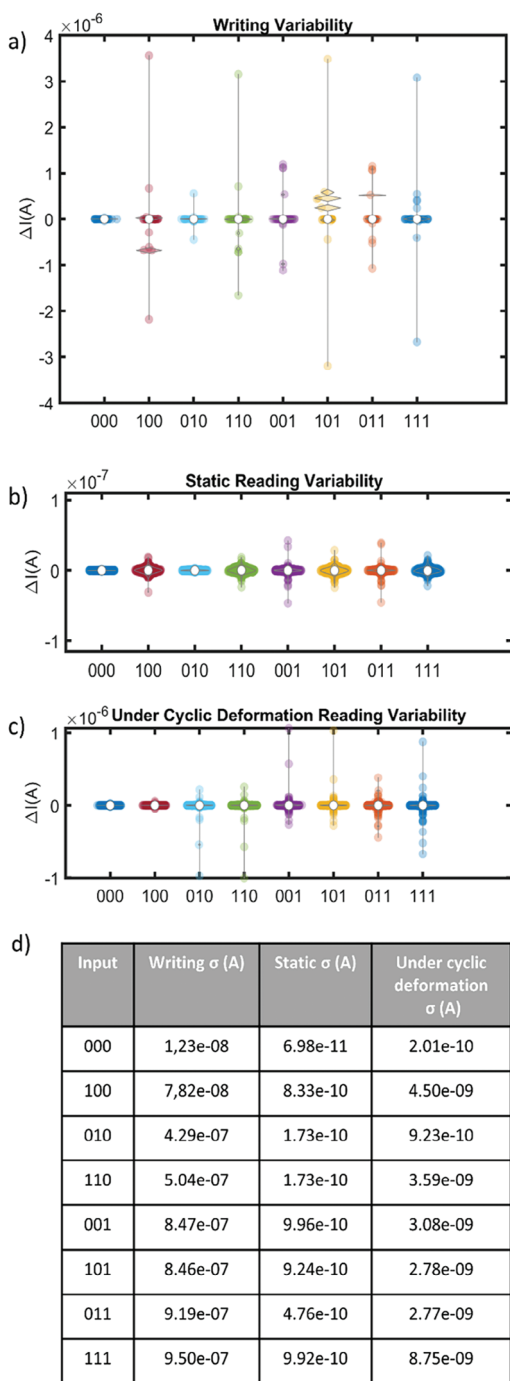
**ADVANCED
SCIENCE NEWS**

www.advancedsciencenews.com

**ADVANCED
ELECTRONIC
MATERIALS**

www.advelectronicmat.de

Figure 8. a) Variability of the measured output currents induced by the writing process, the presence of discrete variations is recurrently observed. b) Variability of the measured output currents observed during the reading phase, the Gaussian-like distributions indicate random variation of much smaller magnitude compared to the effect of the writing phase. c) Variability of the measured output currents observed during the mechanical stability test which evidences the presence of some outliers compared to the static case b). d) Standard deviations relative to the distributions of the variability of the output currents reported in the violin plots. The standard deviations of the static and cyclic mechanical deformation cases, second and third columns respectively, are negligible compared to the variability induced by the writing phase reported in the first column.

network configurations which bring to the same emerging electrical properties. Moreover, the stability of the logic gates under small stress perturbations suggests the possibility of integrating ns-Au/PDMS devices as building blocks of more complex soft computing architectures.

The redundant and adaptive gold nanostructured network, able to spontaneously reconfigure its structure under electrical and mechanical stimuli in a non-deterministic manner, can reproduce a main property of the biological neural network, with its redundant connectivity which realizes through different connected paths resulting in the same significant output. If this resulting electrical response did not lead to the same output through a redundance of possible network configurations, it would not survive the strain impressed by mechanical stimuli. This neuromorphic technology breaks the ranks of the soft implementation of intelligent systems, as in soft robotics and wearable devices framework, to the highest level of intelligence with advanced data processing capabilities.

Our results constitute intelligent matter solutions that would interact with the environment by receiving and responding to external stimuli, while internally adapting their structure to enable the distribution and storage of information. The development of ns-Au/PDMS nanocomposites made by SCBD may be highly proficient for the future realization of bio-inspired neuromorphic platforms integrated in complex unstructured environments, useful for autonomous soft robotics and edge-computing applications.

Supporting Information

Supporting Information is available from the Wiley Online Library or from the author.

Conflict of Interest

The authors declare no conflict of interest.

Data Availability Statement

The data that support the findings of this study are available from the corresponding author upon reasonable request.

[1] M. Li, A. Pal, A. Aghakhani, A. Pena-Francesch, M. Sitti, *Nat. Rev. Mater.* **2021**, *7*, 235.

[2] C. Bartolozzi, G. Indiveri, E. Donati, *Nat. Commun.* **2022**, *13*, 1024.

[3] M. Sitti, *Extreme Mech. Lett.* **2021**, *46*, 101340.

[4] F. Liu, S. Deswal, A. Christou, Y. Sandamirskaya, M. Kaboli, R. Dahiya, *Sci. Robot.* **2022**, *7*, eabl7344.

[5] R. Pfeifer, J. C. Bongard, R. Brooks, *How the Body Shapes the Way We Think: A New View of Intelligence*, The MIT Press, Cambridge, MA, USA **2007**.

[6] C. Hegde, J. Su, J. M. R. Tan, K. He, X. Chen, S. Magdassi, *ACS Nano* **2023**, *17*, 15277.

[7] W. Z. Khan, E. Ahmed, S. Hakak, I. Yaqoob, A. Ahmed, *Future Gener. Comput. Syst.* **2019**, *97*, 219.

[8] M. Horowitz, In *2014 IEEE Int. Solid-State Circuits Conf. Digest of Technical Papers (ISSCC)*, IEEE, Piscataway, NJ **2014**, pp. 10–14.

[9] R. L. Truby, *Acc. Mater. Res.* **2021**, *2*, 854.

[10] D. J. Preston, P. Rothemund, H. J. Jiang, M. P. Nemitz, J. Rawson, Z. Suo, G. M. Whitesides, *Proc. Natl. Acad. Sci. U.S.A.* **2019**, *116*, 7750.

[11] A. Dathbun, S. Kim, S. Lee, D. K. Hwang, J. H. Cho, *Mol. Syst. Des. Eng.* **2019**, *4*, 484.

[12] K. Roztocki, V. Bon, I. Senkovska, D. Matoga, S. Kaskel, *Chem. A Eur. J.* **2022**, *28*, 202202255.

[13] W. Xu, Z. Liu, J. Zhao, W. Xu, W. Gu, X. Zhang, L. Qian, Z. Cui, *Nanoscale* **2014**, *6*, 14891.

[14] G. Corbelli, C. Ghisleri, M. Marelli, P. Milani, L. Ravagnan, *Adv. Mater.* **2011**, *23*, 4504.

[15] L. Migliorini, T. Santaniello, A. Falqui, P. Milani, *ACS Appl. Nano Mater.* **2023**, *6*, 8999.

[16] L. Migliorini, T. Santaniello, S. Rondinini, P. Saettone, M. Comes Franchini, C. Lenardi, P. Milani, *Sens. Actuators, B.* **2019**, *286*, 230.

[17] L. Migliorini, C. Piazzoni, K. Pohako-Esko, M. Di Girolamo, A. Vitaloni, F. Borghi, T. Santaniello, A. Aabloo, P. Milani, *Adv. Funct. Mater.* **2021**, *31*, 2102180.

[18] L. Migliorini, T. Santaniello, F. Borghi, P. Saettone, M. Comes Franchini, G. Generali, P. Milani, *Nanomaterials* **2020**, *10*, 2062.

[19] G. Nadalini, F. Borghi, T. Košutová, A. Falqui, N. Ludwig, P. Milani, *Sci. Rep.* **2023**, *13*, 19713.

[20] G. Martini, M. Mirigliano, B. Paroli, P. Milani, *Jpn. J. Appl. Phys.* **2022**, *61*, SM0801.

[21] B. Paroli, G. Martini, M. A. C. Potenza, M. Siano, M. Mirigliano, P. Milani, *Neural Networks* **2023**, *166*, 634.

[22] M. Mirigliano, D. Decastri, A. Pullia, D. Dellasega, A. Casu, A. Falqui, P. Milani, *Nanotechnology* **2020**, *31*, 234001.

[23] M. Mirigliano, F. Borghi, A. Podestà, A. Antidormi, L. Colombo, P. Milani, *Nanoscale Adv.* **2019**, *1*, 3119.

[24] A. Casu, A. Chiodoni, Y. P. Ivanov, G. Divitini, P. Milani, A. Falqui, *ACS Appl. Nano Mater.* **2024**, *7*, 7203.

[25] M. López-Suárez, C. Melis, L. Colombo, W. Tarantino, *Phys. Rev. Mater.* **2021**, *5*, 126001.

[26] H. Jaeger, *Neuromorph. Comput. Eng.* **2021**, *1*, 012002.

[27] H. Jaeger, B. Noheda, W. G. Van Der Wiel, *Nat. Commun.* **2023**, *14*, 4911.

[28] D. Qi, K. Zhang, G. Tian, B. Jiang, Y. Huang, *Adv. Mater.* **2021**, *33*, 2003155.

[29] J. Lin, Z. Peng, Y. Liu, F. Ruiz-Zepeda, R. Ye, E. L. G. Samuel, M. J. Yacaman, B. I. Yakobson, J. M. Tour, *Nat. Commun.* **2014**, *5*, 5714.

[30] R. Rahimi, M. Ochoa, W. Yu, B. Ziaie, *ACS Appl. Mater. Interfaces.* **2015**, *7*, 4463.

[31] H. Yang, Q. Huang, S. Wang, Q. Zong, C. Tan, H. Ye, G. Zhang, *Appl. Surf. Sci.* **2024**, *660*, 159885.

[32] A. Dallinger, K. Keller, H. Fitzek, F. Greco, *ACS Appl. Mater. Interfaces.* **2020**, *12*, 19855.

[33] K. Wegner, P. Piseri, H. V. Tafreshi, P. Milani, *J. Phys. D: Appl. Phys.* **2006**, *39*, R439.

[34] E. Barborini, P. Piseri, P. Milani, *J. Phys. D: Appl. Phys.* **1999**, *32*, L105.

[35] L. Ravagnan, G. Divitini, S. Rebasti, M. Marelli, P. Piseri, P. Milani, *J. Phys. D: Appl. Phys.* **2009**, *42*, 082002.

[36] C. Ghisleri, F. Borghi, L. Ravagnan, A. Podestà, C. Melis, L. Colombo, P. Milani, *J. Phys. D: Appl. Phys.* **2013**, *47*, 015301.

[37] F. Profumo, F. Borghi, A. Falqui, P. Milani, *J. Phys. D: Appl. Phys.* **2023**, *56*, 355301.

[38] S. Radice, F. Profumo, F. Borghi, A. Falqui, P. Milani, *Adv. Electron. Mater.* **2024**, 2400434.

[39] M. Mirigliano, B. Paroli, G. Martini, M. Fedrizzi, A. Falqui, A. Casu, P. Milani, *Neuromorph. Comput. Eng.* **2021**, *1*, 024007.

[40] J. B. Mallinson, S. Shirai, S. K. Acharya, S. K. Bose, E. Galli, S. A. Brown, *Sci. Adv.* **2019**, *5*, eaaw8438.

[41] J. Hochstetter, R. Zhu, A. Loeffler, A. Diaz-Alvarez, T. Nakayama, Z. Kuncic, *Nat. Commun.* **2021**, *12*, 4008.

[42] J. M. Palva, A. Zhigalov, J. Hirvonen, O. Korhonen, K. Linkenkaer-Hansen, S. Palva, *Proc. Natl. Acad. Sci. U.S.A.* **2013**, *110*, 3585.

[43] M. Karsai, K. Kaski, A.-L. Barabási, J. Kertész, *Sci. Rep.* **2012**, *2*, 397.

[44] A. Mazzoni, F. D. Broccard, E. Garcia-Perez, P. Bonifazi, M. E. Ruaro, V. Torre, *PLoS One* **2007**, *2*, e439.

[45] F. Borghi, M. Mirigliano, D. Dellasega, P. Milani, *Appl. Surf. Sci.* **2022**, *582*, 152485.

[46] W. Tarantino, L. Colombo, *Phys. Rev. Research* **2020**, *2*, 043389.

[47] R. T. Sibatov, A. I. Savitskiy, P. E. L'vov, Y. O. Vasilevskaya, E. P. Kitsyuk, *Nanomaterial* **2023**, *13*, 2039.

[48] C. H. Bok, S. J. Woo, C. Wu, J. H. Park, T. W. Kim, *Scientific Reports* **2017**, *7*, https://doi.org/10.1038/s41598-017-12209-6.

[49] H. Zhu, Z. Tang, G. Wang, Y. Fang, J. Huang, Y. Zheng, *APL Materials* **2023**, *11*, https://doi.org/10.1063/5.0149154.

[50] M. Kaiser, *Front. Neuroinform.* **2011**, *57*, 892.

[51] M. Mirigliano, P. Milani, *Adv. Phys.: X* **2021**, *6*, 1908847.

[52] F. Borghi, M. Mirigliano, P. Milani, A. Podestà, in *Toward a Science Campus in Milan*, (Eds: P. F. Bortignon; G. Lodato, E. Meroni, M. G. A. Paris, L. Perini, A. Vicini), Springer International Publishing, Cham, **2018**, pp. 67–80.

2400717 (12 of 12)